

# A General Method of Solution for the Cluster Variation Method in Ionic Solids, with Application to Diffusionless Transitions in Yttria-Stabilized Zirconia

D.S. Mebane · J.H. Wang

Received: 10 February 2009 / Accepted: 5 April 2010 / Published online: 20 April 2010  
© Springer Science+Business Media, LLC 2010

**Abstract** A new, general method of solution for the cluster variation method using a reduced conjugate gradient approach with a truncated line-search algorithm is presented. The method is generally convergent. Additionally, the truncation of the line-search algorithm may increase the speed of convergence considerably, as the size of the problem is progressively reduced (especially for strongly ordered phases), opening up the possibility of a considerable increase in the size of maximal clusters. The method is successfully demonstrated for a single, eight-atom maximal cluster in the fluorite lattice. Using pairwise defect interaction energies calculated for cubic, yttria-doped zirconia and fixed defect concentrations, a pair of metastable states are found in a composition and temperature range which is experimentally characterized by metastable, diffusionless phase transitions.

**Keywords** Cluster variation method · Reduced gradient method · Yttria-stabilized zirconia · Diffusionless phase transition

## 1 Introduction

The cluster variation method (CVM) is a well-studied technique used to calculate phase equilibria from first principles. Based on the variational principle of statistical mechanics, the method breaks a static lattice into a set of overlapping clusters called the basic or maximal clusters. There may be one or several different types of maximal clusters on the lattice,

---

Support for D.S. Mebane provided by the National Science Foundation International Research Fellowship Program, Grant No. 0701145.

This work was further supported by DOE Basic Energy Sciences under Grant No. DE-FG02-06ER15837.

---

D.S. Mebane (✉)

Max Planck Institute for Solid State Research, Heisenbergstr. 1, 70569 Stuttgart, Germany  
e-mail: [mebane@gatech.edu](mailto:mebane@gatech.edu)

J.H. Wang

Department of Chemistry, National Taiwan Normal University, Taipei, Taiwan  
e-mail: [jenghan@ntnu.edu.tw](mailto:jenghan@ntnu.edu.tw)

with the only stipulation being that no maximal cluster can be a subset of any other. In the following, the set of maximal clusters will be called  $\{\beta\}$ .

If interactions among constituents in the lattice are fully encompassed within the maximal clusters, this leads to an exact expression for the lattice Hamiltonian in terms of the probability distributions of maximal clusters  $\{p_\beta\}$ , which are functions of the cluster configurations  $\{s_\beta\}$ . The most important aspect of the method is a closed-form approximation for the configurational entropy in terms of  $\{p_\beta\}$ , which can be derived using set-theoretic arguments. Minimization of the free energy with respect to  $\{p_\beta\}$  then leads to a statistical description of the lattice at thermal equilibrium. The method is commonly applied to the determination of phase diagrams in metallic alloys or other substitutional solutions (including oxides).

In some respects, CVM is inferior to the more explicit calculations that are possible using Monte Carlo simulations. One shortcoming of present formulations of the method is that the range of interactions among lattice sites is limited to those short-range distances contained within the maximal cluster. A related problem is that the size of the vector  $p_\beta$  increases exponentially with the size of  $\beta$ . When combined with the fact that the free energy functional takes a nonlinear (logarithmic) form, which generally can only be solved with a third-order computational complexity, this means that interaction distances beyond a few atomic spacings can quickly rise to a fairly large computational burden. This problem may be particularly acute in ionic solids, where multiple interacting sublattices and long-ranged chemical interactions may force the use of large maximal clusters.

But CVM also has some distinct advantages over Monte Carlo. It directly calculates free energies, whereas only indirect calculations are possible using importance sampling Monte Carlo. CVM can also be used to easily identify metastable states, as will be demonstrated in this paper.

In order to benefit from these advantages in the context of thermodynamic calculations in ionic solids, however, the problems with long-range interactions and high computational loads must be addressed. This work concerns itself primarily with the latter. A new method, presented and demonstrated in this work for the first time, proves to be a convergent and potentially quite efficient method of solution for the general case of CVM.

## 2 Theory

### 2.1 Formulation of CVM in Ionic Solids

The first description of CVM is usually attributed to Kikuchi [13], while the connection between the work of Kikuchi and that of the quasi-chemical methods described by Guggenheim and Bethe was pointed out by Barker [2]. Barker's work also provided a practical algorithm for the calculation of the entropy coefficients, as demonstrated in the work of Sanchez and de Fontaine [28]. But a rigorous mathematical description of CVM was not achieved until the work of Morita, who first described the method as an expansion of entropy cumulants for which there exists a Möbius inversion; the truncation of the expansion at the maximal clusters and the inversion of the resulting truncated summation leads to a closed-form solution [19]. Schlijper later proved (for a particular case, but in such a manner as to suggest that the results might be more general) that with increasing size of the maximal cluster, the estimate of the free energy provided by the CVM monotonously approaches—and in the limit of an infinite maximal cluster, reaches—the exact result in the thermodynamic limit [29]. Concise summaries of Morita's and Schlijper's work have been written by An [1] and Pelizzola [21].

There is no fundamental change in the method when moving from a single lattice to interpenetrating sublattices, and one may simply treat crystal defects (substitutional dopants or vacancies, or interstitial ions) in exactly the same manner as one treats the components of a metallic alloy [30]. The resulting variational statement is:

$$\begin{aligned}
 F &= \min_{\{p_\beta\}} \mathcal{F}(\{p_\beta\}) \\
 &= \min_{\{p_\beta\}} \sum_{\beta} \left[ \sum_{s_\beta} l_\beta(s_\beta) p_\beta(s_\beta) h_\beta(s_\beta) / k_B T \right. \\
 &\quad \left. + \sum_{\alpha \subseteq \beta} a_\alpha n_\alpha \sum_{s_\alpha} l_\alpha(s_\alpha) p_\alpha(s_\alpha) \log p_\alpha(s_\alpha) \right] \tag{1a}
 \end{aligned}$$

where

$$C_\beta p_\beta = b_\beta \quad \forall \beta \tag{1b}$$

In (1a), which refers to the canonical ensemble,  $F$  is the equilibrium Helmholtz free energy per site (or per chemical formula), which is the minimum of the functional  $\mathcal{F}$  subject to the constraints,  $l_\beta(s_\beta)$  is the degeneracy of the configuration  $s_\beta$ ,  $h_\beta$  is a cluster-specific element of the Hamiltonian, such that  $\mathcal{H}(s_\beta) = \sum_{\beta, s_\beta} h_\beta(s_\beta)$  is the system Hamiltonian (evaluated per site or chemical formula),  $\alpha$  is any subcluster of the maximal cluster  $\beta$ , and  $n_\alpha$  is the number of distinct copies of  $\alpha$  contained in the lattice per site or chemical formula. The coefficients  $a_\alpha$  are integers which may be calculated by analyzing the overlap between the cluster  $\alpha$  and all clusters in the lattice containing it which are also contained in  $\beta$ ; different methods given by An [1] and Sanchez and de Fontaine [28] are equivalent for this purpose. Because the probability distribution  $p_\alpha$  of any subcluster  $\alpha$  of  $\beta$  is a partial sum of  $p_\beta$ , the entropy term in (1a) may be written in terms of  $p_\beta$ .

The constraints on the system given by (1b) are linear— $C_\beta$  is the constraint matrix, which is of size  $M \times N$ , where  $M$  is the number of constraints and  $N$  is the size of the column vector  $p_\beta$ , and  $b_\beta$  is a column vector of length  $M$ . Every application of the method has at least one constraint, which is the normalization criterion,

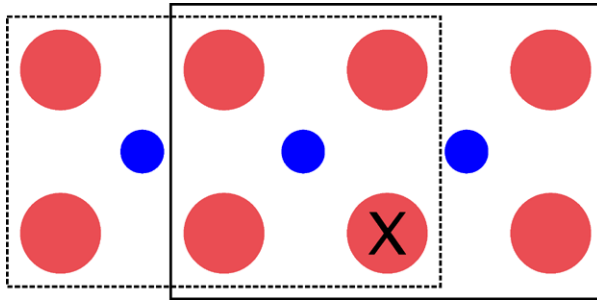
$$\sum_{s_\beta} l_\beta(s_\beta) p_\beta(s_\beta) = 1 \quad \forall \beta \tag{2}$$

In addition, there may be two other types of constraints: concentration constraints and translational constraints. The former may be used in a situation wherein long-range diffusion is kinetically prevented, but short-range re-arrangement of atoms or ions may still take place, such as is frequently the case in diffusionless transformations. The corresponding constraint is:

$$\sum_{s_\beta} l_\beta(s_\beta) p_\beta(s_\beta) n_{f,q}(s_\beta) / n_{t,q}(\beta) = \gamma_q \quad \forall q, \beta \tag{3}$$

where  $\gamma_q$  is the fixed site fraction for the species  $q$ ,  $n_{f,q}(s_\beta)$  is the number of occupied sites of the species  $q$  in  $s_\beta$ , and  $n_{t,q}(\beta)$  is the total number of sites available to species  $q$  in the cluster  $\beta$ .

The translational constraints (also called consistency constraints) arise from the requirement that the maximal clusters remain translationally invariant: subclusters appearing in a



**Fig. 1** Implications of the translational invariance of clusters. *Solid and dotted lines* encapsulate two overlapping clusters on a body-centered square lattice with two distinct sublattices; it is clear that the single site marked with an “X” (along with other sites and subclusters of the maximal cluster) inhabits a different environment in each. Nevertheless, its occupancy probability must be the same for each main cluster

maximal cluster which are equivalent in the lattice must have equivalent probability distributions, even when they occupy inequivalent positions within the maximal clusters. Figure 1 illustrates the situation for an eight-site maximal cluster on a two-dimensional body-centered square lattice with interpenetrating sublattices. The marked site occupies symmetrically inequivalent positions in the two overlapping maximal clusters shown, but of course the marked site may possess only one occupancy probability. The probability distribution for the maximal cluster must therefore reflect the same occupancy probability for sites at the ends of the figure as for sites in the middle. Because the distribution of each subcluster is normalized and the set of subclusters of the maximal cluster is partially ordered, this can be accomplished in a binary alloy by requiring merely that the probability distribution of the fully occupied subclusters are equivalent. The corresponding constraint statements are:

$$\sum_{s_{\beta_i}} I_{\beta_i}(s_{\beta_i}) p_{\beta_i}(s_{\beta_i}) n_{o,i}(s_{\beta_i}) / n_{c,i}(\beta_i) = \sum_{s_{\beta_j}} I_{\beta_j}(s_{\beta_j}) p_{\beta_j}(s_{\beta_j}) n_{o,j}(s_{\beta_j}) / n_{c,j}(\beta_j) \quad (4)$$

$$\forall (i \subset \beta_i, j \subset \beta_j), \beta_{i,j} \in \{\beta\}$$

where  $n_{o,i}(s_{\beta_i})$  is the number of fully occupied subclusters and  $n_{c,i}(s_{\beta_i})$  the total number of subclusters of a given type  $i$  occurring in the maximal cluster configuration  $s_{\beta_i}$ , and  $i, j$  denote subcluster types that are symmetrically equivalent in the full crystal but inequivalent in the maximal clusters  $\beta$ .

## 2.2 Method of Solution and Implementation

### 2.2.1 Reduced Gradient Method

Deriving a general, provably convergent method of solution for this problem can be quite straightforward. Given the linearity of the constraints, one may simply incorporate them into the formulation of the functional, thereby reducing the problem to one of unconstrained optimization. This avails the problem to methods of the steepest descent/conjugate gradient type.

One strategy for reducing the problem is a linear transformation of the probability distribution into a space in which the constraints are automatically satisfied. Such a transformation was derived by Sanchez and de Fontaine, which converts the vector  $p$  (we will leave off

all subscripts  $\beta$  for the remainder of this section) into a smaller vector  $\xi$ , whose elements are the  $n$ -point correlation functions for all of the distinct subclusters of the maximal clusters [28]. Concentration constraints are satisfied simply by fixing the appropriate one-point correlations. The difficulty with this method, however, is that the transformation distorts the boundary of the function space—instead of a cuboid bounded at 1 and 0 in each dimension as it is in  $p$ -space, the allowable range of the probability function becomes a polyhedron in  $\xi$ -space, potentially introducing machine error into the specification of the boundary.

The reduced gradient method (see, for example, Ref. [27]), by contrast, requires no transformation of the function space, instead directly reducing the size of the problem by establishing subsets of dependent and independent variables, related through the constraint matrix. In this method, the constraint matrix  $C$  is split into two submatrices  $B$  and  $S$ , such that  $C = [B \ S]$  with nonsingular  $B$  of size  $M \times M$ . The vector  $p$  is split into two corresponding subvectors,  $p_B$  and  $p_S$ , such that

$$Bp_B = b - Sp_S \tag{5}$$

The relationship between the corresponding descent vectors  $\delta_B$  and  $\delta_S$  is

$$B\delta_B = -S\delta_S \tag{6}$$

We may then write the total derivative of the functional  $\mathcal{F}$  with respect to the independent variables as:

$$D_S \mathcal{F} = \nabla_S \mathcal{F} - S^T (B^{-1})^T \nabla_B \mathcal{F} \tag{7}$$

If a gradient-based method is used, it follows that each step of the process will require an inversion of the matrix  $B$ . However, the dimensions of  $B$  are likely to be much less than the length of  $p$ , with the discrepancy generally increasing with the size of the basic cluster. Also, so long as  $B$  does not change, we may decompose it at the outset (a  $QR$ -decomposition was used) and store the decomposed matrix. The dependent variables can be any which yield a nonsingular  $B$ . Using (1)–(4) and (7), any gradient-based method for unconstrained optimization can be applied. The algorithm used in this work was the Polak-Ribière conjugate gradient method (see Ref. [9]).

Bracketing of the line search along the direction of descent is quite natural, taking advantage of the form of the functional and the dimensions of the function space. These dimensions are established by the fact that each element  $p(s)$  must have a value on the interval  $(0, 1)$ . If a descent direction has been found, the (infinitely) positive gradient of the functional along any direction as the boundary is approached guarantees the existence of a directional minimum between the starting point and the boundary. If a descent direction cannot be found, then the routine is at a stationary point.

### 2.2.2 Line Search Cutoff

In a typical application of the method using a basic cluster of appreciable size and realistic cluster energies (such as those based on quantum calculations), many of the elements of  $p_\beta$  will become very small—the higher the degree of ordering, the smaller the proportion of elements of  $p_\beta$  that will contribute to the statistical description of the stable state. If one could identify a set of basic cluster configurations that are likely to have appreciable probabilities at a given temperature and concentration, the size of the problem could often be reduced considerably.

One strategy for doing this is to designate as “dormant” elements of  $p_\beta$  which shrink beyond a certain threshold during the course of the line search, terminating the line search

and calculating a new descent direction without considering the dormant terms. One must, of course, allow for the possible “reawakening” of dormant elements. This is best accomplished when the problem has reached a convergence point—when the norm of the gradient reaches a certain absolute or relative value. A full gradient is then calculated, including a full set of independent variables. Any dormant elements that would be forced further toward zero in the new search direction remain dormant, but the others are reactivated. The cycle of convergence and reactivation continues until none of the dormant elements of a converged set reactivate.

Formally, the criterion used in the line search was

$$\|f(x)\| < -0.1 f'(0) \vee \exists s_{\beta}^* : p_{\beta}(s_{\beta}^*, x) < \tau_l \quad (8)$$

where  $f$  is the value of the functional,  $f'$  is the directional derivative along the line of descent,  $x$  is the distance from the starting position,  $\tau_l$  is the cutoff level, and  $s_{\beta}^*$  indicates an active configuration. If the latter criterion was met first, the configuration leading to the cutoff was made dormant, and a new steepest descent direction was calculated for the remaining active configurations.

### 2.2.3 Implementation

Some further comments on the implementation are in order. In the successive shrinking of the number of active elements, one effectively eliminates columns from the matrix  $C$ , leading to a reduced matrix  $C_r$ . This means that mechanisms must be in place to ensure that a full-rank matrix  $B$  can be found when columns in the current  $B$  are eliminated. So long as the matrix  $C_r$  is full-rank, this will always be possible (for example, through the formation of the row-echelon matrix for  $C_r$ , which is the method used in this work). But when the rows of  $C_r$  become linearly dependent, one or more rows (and along with them the corresponding constraints) must also go dormant. The linear independence of the rows of  $C_r$  was monitored at each re-establishment of the matrix  $B$ , by calculating the eigenvalues and eigenvectors of  $C_r C_r^T$  using Jacobi rotation (a step with  $\mathcal{O}(N^2)$  complexity). A related issue is that occasionally more than one element will approach zero simultaneously; when this happens, all of these elements must go dormant at once.

Finally, either the elimination or the reactivation of elements may lead to a situation in which very small dependent elements are “pushed” over the boundary to zero or negative values due to roundoff errors. One must therefore establish a failsafe routine which can reset the small independent variables in such a way that the dependent set is all positive. For this purpose, an iterative process was established, wherein the whole set is moved in such a way as to minimize the movement of elements while bringing all elements into the allowable range. Such a routine can also handle many of the problems with roundoff error which are bound to arise in the calculation of dependent variables.

## 3 Application

### 3.1 Metastable Transitions in YSZ

YSZ is a very important functional ceramic, used in gas sensors and as an electrolyte in solid oxide fuel cells. At temperatures less than 1000°C and for concentrations of yttrium above a few percent, the conductivity in YSZ is almost completely ionic. The mechanism

for the conductivity is the motion of oxygen ions through the bulk of the material, a process which may just as well be characterized by the motion of oxygen vacancies through the lattice. These vacancies are created as electrostatic compensation for aliovalent yttrium atoms, which substitute for zirconium, creating an effectively negatively-charged defect.

In pure and yttrium-doped zirconia with compositions of  $YO_{1.5}$  less than approximately 35 mol %, there are three equilibrium phases: the monoclinic, tetragonal and cubic solid solutions [8]. The monoclinic is the low-temperature phase of pure zirconia, and the tetragonal and cubic phases are realized at progressively higher temperatures by way of martensitic (diffusionless and displacive) transformations. Addition of yttria thermodynamically stabilizes both tetragonal and cubic phases at lower temperatures. But for finite concentrations of yttrium, the equilibrium phase transformations are accompanied by yttrium diffusion.

However, the very slow cation mobility in doped zirconias can prevent the formation of the equilibrium monoclinic and tetragonal phases, creating instead a number of metastable phases realized through diffusionless phase transitions [32]. At low yttrium concentrations (approximately less than 3 mol %), transitions between metastable tetragonal and monoclinic phases are martensitic in nature and stress-induced at low temperature, and have been widely studied due to the increase in fracture toughness associated with these transitions [12]. At higher concentrations of yttrium, there are a pair of irreversible, metastable, diffusionless cubic-to-tetragonal transitions (often noted as  $c - t'$  and  $c - t''$ ) [6, 26, 32, 33], which are realized by rapidly quenching from the melt.

CVM, with its ability to identify metastable states and a natural ability to control local concentration through constraints on the minimization, could be useful in the study of such metastable transitions.

### 3.2 Maximal Clusters

For the case of the fluorite lattice, a single maximal cluster was chosen, shown in Fig. 2. It has six cation positions encasing one nearest-neighbor anion pair, for a total of eight ions in all. It can be viewed as a pair of adjacent, edge-sharing cation tetrahedra along with the enclosed anion of each. This cluster, from here on referred to as the 8-figure, was chosen for convenience, along with its potential utility in estimating vacancy transport properties in doped fluorite oxides—it has been used by different investigators for this purpose [20, 23].

For a system with binary occupancy on both sublattices, there are 512 different configurations of the 8-figure, of which, however, only 72 are nondegenerate. An's result for finding the coefficients  $a_\alpha$  (without recourse to the corresponding Möbius function) can be written

$$\sum_{\substack{\alpha \subseteq \theta \\ \theta \in P}} a_\theta = 1 \quad (9)$$

where  $P$  is the set of clusters formed by  $\beta$  and all of its subclusters found throughout the lattice. The breakdown of relevant subclusters and coefficients  $a_\beta$  is given in Fig. 3.

Translational analysis of the 8-figure reveals a number of subclusters that are crystallographically equivalent in the fluorite lattice but inequivalent in the 8-figure. These clusters are shown in Fig. 4; among them eight different constraints are required to ensure the translational invariance of the 8-figure probability distribution. Along with concentration constraints on both sublattices and normalization, this leads to eleven constraint equations overall: the dimensions of the matrix  $C$  are  $11 \times 72$ .

The usual procedure is to use the free energy functional of (1a) to calculate the grand potential, which leads to identification of phases and their boundaries in the equilibrium phase

**Fig. 2** The maximal cluster used in the study. The cluster contains two anions and six cations; it is effectively two edge-sharing cation tetrahedra, along with the central anions of each. The plane shown in the figure is the (110)

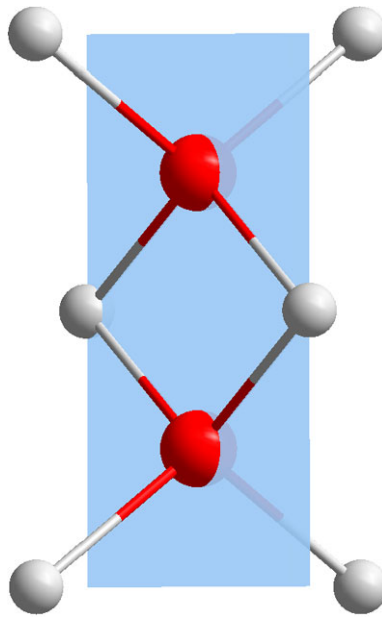


diagram. In a situation wherein the concentrations are fixed, however, one must minimize the Helmholtz energy, meaning that (1) is the final statement of the problem in the present case.

### 3.3 Energies

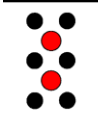

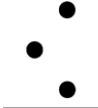
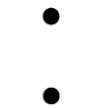


For simplicity, we calculate the Hamiltonian in a pairwise fashion, despite evidence to suggest that the actual situation in YSZ is more complicated than this [4, 5, 10, 24]. Utilizing more complete information on the defect interaction energies in YSZ would likely require a larger maximal cluster (and possibly a mean-field accounting for long-range Coulomb interactions). The pair interactions utilized are listed in Table 1, along with energies taken from the work of Pornprasertsuk et al. [23]. Pornprasertsuk and co-authors used density functional theory to calculate the overall energies of supercells containing 36 cation sites and 72 anion sites, among which there were 6 yttrium ions and 3 oxygen vacancies. The data in Table 1 for the energies of various defect pairs were acquired using a least-squares fitting. The data appearing in the table are incomplete, as Pornprasertsuk et al. calculated Y-Y and V-V interactions up to fourth nearest neighbor. However, interaction energies for Y-Y beyond second nearest neighbor were fairly low, while the maximal cluster used in this study does not contain Y-V relationships beyond second nearest neighbor. Pornprasertsuk et al. did not calculate energies for V-V interactions; these were supplied by our own DFT calculations (like Pornprasertsuk et al., we used a plane wave basis set, the generalized gradient [7, 22] and projector-augmented wave [3, 18] methods, and the Vienna *Ab Initio* Simulation Package [16–18] on  $2 \times 2 \times 2$  supercells), which suggested that the energy for a first nearest neighbor V-V interaction is in the neighborhood of 1.0 eV.

### 3.4 Stability and Performance of the Method

The code was written in C++, using the Blitz++ container class [31].



**Fig. 3** The subclusters and coefficients that enter into the approximation of the entropy for the fluorite lattice with a maximal cluster as shown in Fig. 2, when each sublattice has a binary occupation. Here, in accordance with (1a),  $n_\alpha$  is the number of each subcluster found in the lattice per cation site, and  $a_\alpha$  is the entropy coefficient

$\alpha$	$n_\alpha$	$a_\alpha$
	6	1
	2	-5
	12	-1
	3	1
	6	4
	1	-13

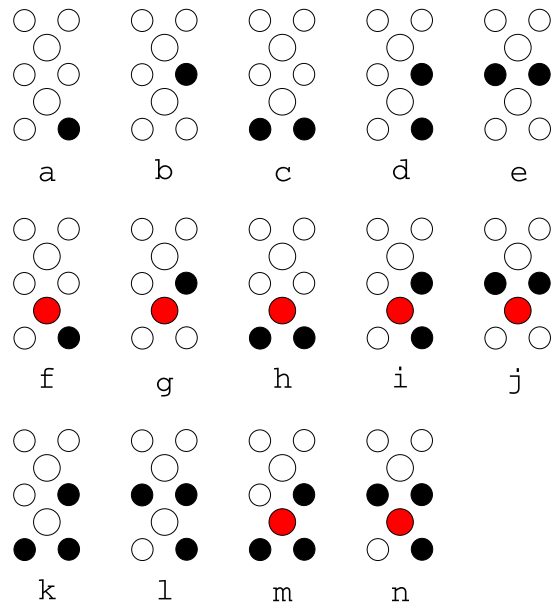
**Table 1** Bond energies for various defect pairs

Bond	Energy (eV)
Y-Y 1NN	0.0335
Y-Y 2NN	0.1451
V-V 1NN	1.0
Y-V 1NN	-0.2988
Y-V 2NN	-0.3531

The solution method was tested using the energies listed in Table 1, in the composition range 0.05–0.35 mol % YO<sub>1.5</sub> and 400–2000 K. The performance was generally quite good, with a 97.3% success rate. Those cases which did not converge likely owe their failure to machine error-related problems; further improvements to the code could push the success rate up close to 100%.

There are two measures of tolerance built into the code: the convergence tolerances  $\tau_r$  and  $\tau_a$  and the line search cutoff tolerance  $\tau_l$ . The former is a test of the  $L_2$ -norm of the reduced gradient (7), and the routine was found to be tolerably stable for the test runs at an absolute value  $\tau_a = 10^{-4}$  and relative value  $\tau_r = 10^{-6}$ . For the test runs, the method was found to be relatively insensitive to  $\tau_l$  in terms of finding local minima. The tradeoff here

**Fig. 4** Subclusters involved in the constraints for translational invariance. The constraints correspond to  $a \equiv b$ ,  $c \equiv d$ ,  $c \equiv e$ ,  $f \equiv g$ ,  $h \equiv i$ ,  $h \equiv j$ ,  $k \equiv l$  and  $m \equiv n$



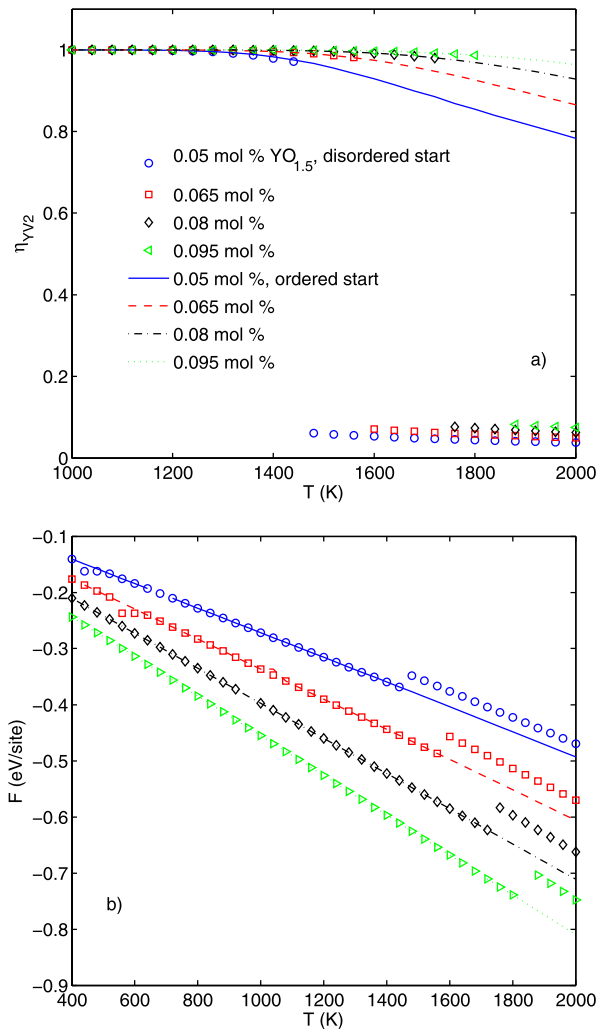
is speed vs. accuracy—the solution is only as accurate as the size of  $\tau_l$  (which cannot be smaller than the machine precision). In order to be certain of an accurate result,  $\tau_l = 10^{-10}$  was used, although a tolerance several orders of magnitude greater would probably have been acceptable.

Using these tolerances, speed of convergence was, depending on the start point and final phase reached, anywhere between several seconds and a fraction of a second on a single CPU of an Intel Core2Duo processor. Unsurprisingly, convergence to metastable states took longer than convergence to stable ones. In terms of iterations, the average number for successfully converged runs was 4595, with a standard deviation of 9010 and median of 1507. These numbers reflect the sensitivity of the computation time to the starting point and to the nature of the local minimum reached; on the runs with higher iteration counts, much time was spent toward the end of the run in the neighborhood of the minimum, suggesting that second-order information might be used to speed things up considerably. However, even as it stands, the time to convergence was quite reasonable, suggesting room for considerable increase in the size of the maximal cluster.

### 3.5 Metastable Order-Disorder Transitions

A set of order parameters for the system was established in the following way. From the converged probability distributions at each state point, the likelihood of occurrence of the defect pairs used in the Hamiltonian were calculated. We will call this set of probabilities  $\{x_{i,j}\}$ , where the index  $i$  refers to the particular pair, one of YY1 (first nearest-neighbor yttrium pair), YY2, YV1 (first nearest-neighbor yttrium-vacancy pair), YV2 or VV, and the index  $j$  (if applicable) refers to the phase. Two phases that can be identified right away based only upon the Hamiltonian, the crystal structure and the concentrations are the completely random phase—the maximization of the entropy assuming no defect interactions—and the completely ordered phase, which is found by minimizing the Hamiltonian subject to the constraints of concentration, normalization and translational invariance. Denoting these phases

**Fig. 5** **a** order parameter for second-nearest neighbor yttrium-vacancy separations and **b** corresponding free energies for state points calculated at 40-degree intervals between 400 and 2000 K and concentrations of 0.05–0.095 mol % YO<sub>1.5</sub>. *Discrete symbols* indicate that the starting point was the completely random state; the starting point for the *solid lines* was the completely ordered state. The deviations from a smooth line in the free energy at 0.065 mol % in the neighborhood of 600 K are due to a slight numerical instability



with the subscripts  $j \equiv o$  and  $j \equiv r$ , respectively, we may calculate the order parameters  $\eta_i$  in the following way:

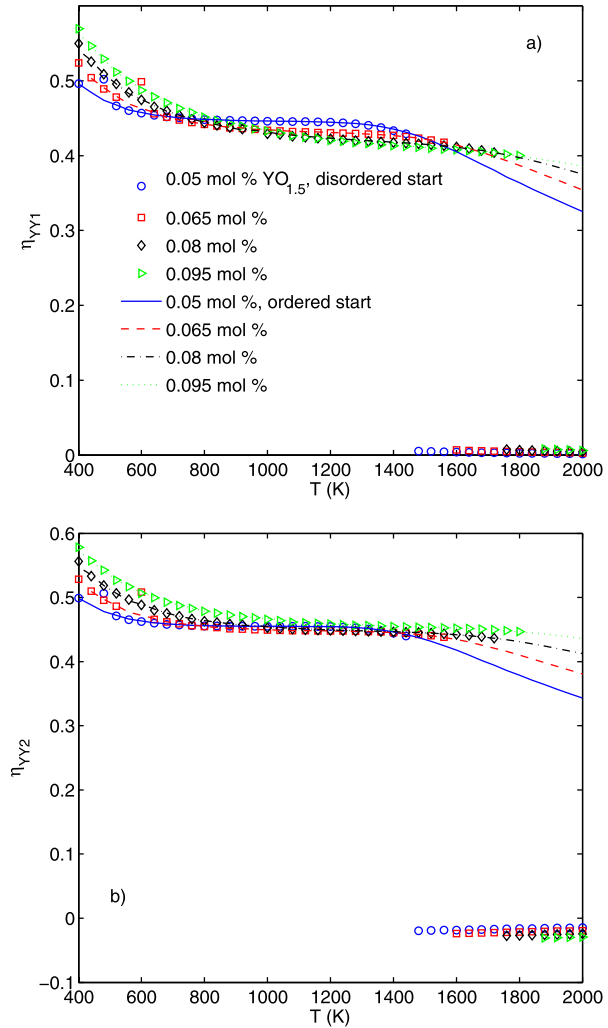
$$\eta_i = \frac{x_i - x_{i,r}}{x_{i,o} - x_{i,r}} \tag{10}$$

A plot of  $\eta_{YV2}$  for temperatures in the range 1000–2000 K and doping fractions of 0.05–0.095 mol % YO<sub>1.5</sub>, along with a plot of the corresponding free energies, are shown in Fig. 5, with plots for  $\eta_{YY1}$  and  $\eta_{YY2}$  appearing in Fig. 6.

Two stable phases appear for this system—a relatively ordered phase, whose principal components in terms of the 8-figure are shown in Fig. 7, and a relatively disordered phase occurring at high temperatures, in which many different 8-figure configurations have a significant probability.

As the free energies reveal, however, the disordered phase is only metastable, and convergence to this phase depends on the starting point in the optimization. Two different starting

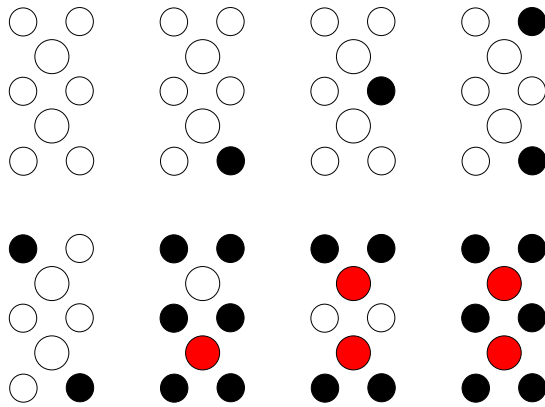
**Fig. 6** Order parameters for **a** first and **b** second-nearest neighbor yttrium-yttrium separations for state points calculated at 40-degree intervals between 400 and 2000 K and concentrations of 0.05–0.095 mol %  $\text{YO}_{1.5}$ . *Discrete symbols* indicate that the starting point was the completely random state; the starting point for the *solid lines* was the completely ordered state



points were used, corresponding to the completely random and completely ordered phases discussed above. It was only possible to realize the diffuse phase when starting from the random distribution. When starting from the completely ordered state, the ordered phase is always found, as indicated by the continuous lines in Figs. 5 and 6. As temperatures decrease, the disordered phase becomes unstable. These transition points between metastability and instability were determined to within 1 K for each concentration by tightening tolerances to  $\tau_r = 10^{-7}$  and  $\tau_a = 10^{-5}$ , stepping down in temperature in single-degree increments, and using the convergence point for the previous step as the starting point for the next. (It should be pointed out that the error in determination of critical temperatures using this method may be greater than 1 K.) The results appear in Table 2.

It is clear that these calculations, in requiring that the concentration of defects in the phase remain constant, correspond in some sense to those situations in which the long-range diffusion required in nucleation and growth processes is restricted. The diffusion distances allowed are probably not more than one or two inter-cation spacings. From Fig. 7, it seems

**Fig. 7** Configurations of the 8-figure which appear in the ordered phase



**Table 2** Transition temperatures at which the disordered phase becomes unstable for various concentrations of yttrium

Concentration (mol % YO <sub>1.5</sub> )	Transition temperature (K)
0.05	1452
0.065	1591
0.08	1725
0.095	1855

that the effect of the ordering reaction could be a short-range clustering of yttrium—perhaps in groups spanning only a portion of a unit cell—separated by areas of relatively sparse defect concentration. In any event, it is worth reiterating that the “equilibrium” phase calculated here is in fact also metastable with respect to the given Hamiltonian and crystal structure.

As mentioned, the disordered phase is only visited (for the state points for which it is stable) when the starting point is also disordered—this simulates a rapid quench from high temperature, but of course in reality the appearance of such a metastable phase depends on the energy barrier between it and the more stable alternative, compared with the amount of thermal energy in the system. In this sense, the descent method, which allows defects to move only in the direction of a decrease in free energy, is in fact a poor model of the physical behavior—it can be used to identify potentially stable states, but not to predict whether or not they will actually occur.

With this caveat, and cognizant of the likely shortcomings of the Hamiltonian, we compare the transitions calculated with those of the experimental metastable phase diagram constructed by Yashima et al. [32]. In Yashima’s diagram, there are, in fact,  $c - t'$  and  $c - t''$  transitions occurring in the temperature and concentration range where the diffuse phase was found to be stable in the present study. But the behavior with respect to temperature and concentration is opposite: additional yttrium tends to stabilize the high-temperature cubic phase in the experimental system, whereas addition of yttrium tends to destabilize the high-temperature phase in this study, as shown in Figs. 5 and 6 and Table 2. Given the simplified nature of the Hamiltonian, the size of the maximal cluster, and the fact that all energy calculations were made in cubic phases, it is difficult to comment on this discrepancy. However, in reference to the discussion of the previous paragraph, it could be pointed out that the increase in thermal energy afforded by the higher temperatures might be the decisive factor here.

### 4 Discussion

One of the oldest and perhaps most widely used methods of solution for CVM is Kikuchi’s natural iteration method (NIM) [14, 15]. As the name suggests, this method has the advantage of a very straightforward implementation. The constraints are added to the functional with Lagrange multipliers. The functional is then differentiated with respect to  $p_\beta(s_\beta)$ , and  $p_\beta(s_\beta)$  is solved for in terms of its subcluster marginals  $p_\alpha$ ,  $\alpha \subset \beta$  and the Lagrange multipliers:

$$p_\beta(s_\beta) \propto \exp \left[ \frac{-h_\beta(s_\beta)}{n_\beta k_B T} \right] \left\{ \prod_k \exp [\lambda_k(\beta) L_\beta(s_\beta)] \right\} \prod_{\alpha \subset \beta} \prod_{s_\alpha} p_\alpha(s_\alpha)^{L_{\alpha\beta}(s_\alpha, s_\beta)} \quad (11)$$

where  $\lambda_k$  are the Lagrange multipliers, and  $L_\beta$  and  $L_{\alpha\beta}$  are sets of constants depending on the lattice and choice of maximal clusters. The main iteration, beginning with a guess  $\{p_\beta(s_\beta)\}$ , successively calculates the subcluster marginals and a new  $\{p_\beta(s_\beta)\}$  through (11). The inner loop of the iteration is one in which Lagrange multipliers must be solved for by substituting (11) into the constraint equations (2)–(4). Newton’s method may be used for this inner loop, or some other iterative scheme.

Pretti [25] analyzed the NIM in its general form, and determined a sufficient criterion for the convergence of the outer loop, which depends on the form of the lattice and maximal clusters through the coefficients  $c_\alpha = a_\alpha n_\alpha$ . The criterion states that, for all maximal clusters  $\beta$ , there exists a set of nonnegative coefficients  $\{c_{\alpha-|\alpha^+}\}$  such that

$$c_{\alpha^+} = \sum_{\alpha^+ \subset \alpha^- \subset \beta} c_{\alpha^-|\alpha^+} \quad \forall \alpha^+ \subset \beta \quad (12a)$$

$$-c_{\alpha^-} \geq \sum_{\alpha^+ \subset \alpha^-} c_{\alpha^-|\alpha^+} \quad \forall \alpha^- \subset \beta \quad (12b)$$

where  $\alpha^+$  and  $\alpha^-$  denote subclusters with positive and negative coefficients  $c_{\alpha^+}$  and  $c_{\alpha^-}$ , respectively. An analysis linking Pretti’s criterion with the form of the lattice and maximal clusters has not yet appeared. However, one may verify that the basic cluster used in Sect. 3 does not meet this criterion.

Pretti also showed that NIM is a special case of a general class of methods for solving CVM problems. These methods were presented in general form by Heskes et al. [11], who expanded on the work of Yuille [34]. The main idea is the splitting of the CVM functional into concave and convex parts. The more general method given by Heskes et al. re-writes the problem in a fully convex form, by bounding from above the concave parts of the functional with a convex one at each iteration. Belief propagation can then be reliably used to minimize the convex functionals.

These belief propagation-based algorithms (including NIM) are not subject to failure due to roundoff errors in the calculation of the basic cluster marginals  $p_\beta(s_\beta)$ . This is because they all take the form of (12) in the sense of being a product of positive terms, thereby ensuring that all probabilities are greater than zero. This is a relative advantage over the method presented in this paper in terms of reducing the complexity in implementation, considering the various measures needed for the implementation of the reduced gradient method as described in Sect. 2.2.3.

However, like the belief propagation/bounding methods, the reduced gradient/line search cutoff method is provably convergent for the general case. Its principal advantage over other methods is its winnowing of the size of the problem, meaning that it will probably be most

appropriate to use in the case of complex, low-symmetry lattices and large maximal clusters. Use of the method in these contexts could help CVM retain its advantage in computational load over Monte Carlo methods.

## 5 Conclusion

The reduced gradient method with a line search cutoff is a generally convergent method of solution for the cluster variation method, in which the computational load for problems in complex lattices with large maximal clusters may be considerably reduced. The routine was tested successfully on an eight-ion cluster in a fluorite lattice, with binary occupancy on each sublattice. Using pairwise energies calculated using DFT models of yttria-doped cubic zirconia, the method located metastable disordered phases at high temperatures and low doping levels.

**Acknowledgements** D.S.M. would like to acknowledge Profs. Joachim Maier and Eugene Kotomin for helpful input, and especially Prof. Meilin Liu for his advice and support over the course of this project.

## References

1. An, G.Z.: A note on the cluster variation method. *J. Stat. Phys.* **52**(3–4), 727–734 (1988)
2. Barker, J.A.: Methods of approximation in the theory of regular mixtures. *Proc. R. Soc. A* **216**(1124), 45–56 (1953)
3. Blöchl, P.E.: Projector augmented-wave method. *Phys. Rev. B* **50**(24), 17953–17979 (1994)
4. Bogicevic, A., Wolverton, C.: Nature and strength of defect interactions in cubic stabilized zirconia. *Phys. Rev. B* **67**(2), 024106 (2003)
5. Bogicevic, A., Wolverton, C., Crosbie, G.M., Stechel, E.B.: Defect ordering in aliovalently doped cubic zirconia from first principles. *Phys. Rev. B* **64**(1), 014106 (2001)
6. Caracoche, M.C., Martinez, J.A., Rivas, P.C., Rodriguez, A.M., Lamas, D.G., Lascalea, G.E., de Reza, N.E.W.: Hyperfine characterization of the metastable  $t''$ -form of the tetragonal phase in  $\text{ZrO}_2$ —10 mol %  $\text{Y}_2\text{O}_3$  powders synthesized by gel combustion. *J. Am. Ceram. Soc.* **88**(6), 1564–1567 (2005)
7. Ceperley, D.M., Alder, B.J.: Ground-state of the electron-gas by a stochastic method. *Phys. Rev. Lett.* **45**(7), 566–569 (1980)
8. Chen, M., Hallstedt, B., Gauckler, L.J.: Thermodynamic modeling of the  $\text{ZrO}_2$ – $\text{YO}_{1.5}$  system. *Solid State Ion.* **170**(3–4), 255–274 (2004)
9. Fletcher, R.: *Practical Methods of Optimization*, 2nd edn. Wiley-Interscience, New York (1987)
10. Goff, J.P., Hayes, W., Hull, S., Hutchings, M.T., Clausen, K.N.: Defect structure of yttria-stabilized zirconia and its influence on the ionic conductivity at elevated temperatures. *Phys. Rev. B* **59**(22), 14202–14219 (1999)
11. Heskes, T., Albers, K., Kappen, B.: Approximate inference and constrained optimization. In: M. Kaufmann (ed.) *Proceedings of the 19th Annual Conference on Uncertainty in Artificial Intelligence (UAI-03)*, p. 313 (2003)
12. Kelly, P.M., Rose, L.R.F.: The martensitic transformation in ceramics: its role in transformation toughening. *Prog. Mater. Sci.* **47**(5), 463–557 (2002)
13. Kikuchi, R.: A theory of cooperative phenomena. *Phys. Rev.* **81**(6), 988–1003 (1951)
14. Kikuchi, R.: Natural iteration method and boundary free-energy. *J. Chem. Phys.* **65**(11), 4545–4553 (1976)
15. Kikuchi, R., Brush, S.G.: Improvement of cluster-variation method. *J. Chem. Phys.* **47**(1), 195 (1967)
16. Kresse, G., Hafner, J.: *Ab-initio* molecular-dynamics for liquid-metals. *Phys. Rev. B* **47**(1), 558–561 (1993)
17. Kresse, G., Hafner, J.: *Ab-initio* molecular-dynamics simulation of the liquid-metal amorphous-semiconductor transition in germanium. *Phys. Rev. B* **49**(20), 14251–14269 (1994)
18. Kresse, G., Joubert, D.: From ultrasoft pseudopotentials to the projector augmented-wave method. *Phys. Rev. B* **59**(3), 1758–1775 (1999)
19. Morita, T.: General structure of distribution functions for Heisenberg model and Ising-model. *J. Math. Phys.* **13**(1), 115 (1972)

20. Nakayama, M., Martin, M.: First-principles study on defect chemistry and migration of oxide ions in ceria doped with rare-earth cations. *Phys. Chem. Chem. Phys.* **11**(17), 3241–3249 (2009)
21. Pelizzola, A.: Cluster variation method in statistical physics and probabilistic graphical models. *J. Phys. A* **38**(33), R309–R339 (2005)
22. Perdew, J.P., Wang, Y.: Accurate and simple analytic representation of the electron-gas correlation-energy. *Phys. Rev. B* **45**(23), 13244–13249 (1992)
23. Pornprasertsuk, R., Ramanarayanan, P., Musgrave, C.B., Prinz, F.B.: Predicting ionic conductivity of solid oxide fuel cell electrolyte from first principles. *J. Appl. Phys.* **98**(10), 103513 (2005)
24. Predith, A., Ceder, G., Wolverton, C., Persson, K., Mueller, T.: Ab initio prediction of ordered ground-state structures in  $\text{ZrO}_2\text{-Y}_2\text{O}_3$ . *Phys. Rev. B* **77**(14), 144104 (2008)
25. Pretti, M.: On the convergence of Kikuchi's natural iteration method. *J. Stat. Phys.* **119**(3-4), 659–675 (2005)
26. Rodriguez, A.M., Caracoche, M.C., Rivas, P.C., Pasquevich, A.F., Mintzer, S.R.: PAC characterization of nontransformable tetragonal  $t'$  phase in arc-melted zirconia—2.8 mol % yttria ceramics. *J. Am. Ceram. Soc.* **84**(1), 188–192 (2001)
27. Ruszczyński, A.: *Nonlinear Optimization*. Princeton University Press, Princeton (2006)
28. Sanchez, J.M., de Fontaine, D.D.: FCC Ising-model in cluster variation approximation. *Phys. Rev. B* **17**(7), 2926–2936 (1978)
29. Schlijper, A.: Convergence of the cluster-variation method in the thermodynamic limit. *Phys. Rev. B* **27**(11), 6841–6848 (1983)
30. Tepešch, P.D., Garbulsky, G.D., Ceder, G.: Model for configurational thermodynamics in ionic systems. *Phys. Rev. Lett.* **74**(12), 2272–2275 (1995)
31. Veldhuizen, T.L.: Arrays in Blitz++. In: *Computing in Object-Oriented Parallel Environments*. Second International Symposium, ISCOPE 98, pp. 223 (1998)
32. Yashima, M., Kakihana, M., Yoshimura, M.: Metastable-stable phase diagrams in the zirconia-containing systems utilized in solid-oxide fuel cell application. *Solid State Ion.* **86-8**, 1131–1149 (1996)
33. Yashima, M., Sasaki, S., Kakihana, M., Yamaguchi, Y., Arashi, H., Yoshimura, M.: Oxygen-induced structural-change of the tetragonal phase around the tetragonal-cubic phase-boundary in  $\text{ZrO}_2\text{-YO}_{1.5}$  solid-solutions. *Acta Cryst.* **50**, 663–672 (1994)
34. Yuille, A.L.: CCCP algorithms to minimize the Bethe and Kikuchi free energies: Convergent alternatives to belief propagation. *Neural Comput.* **14**(7), 1691–1722 (2002)